

Development of non-fluorinated superhydrophobic and cytocompatible polymer coatings

Erta Petsi^{a,b}, Franceska Gojda^{a,c}, Fanourios Krasanakis^a, Abeer Shaalan^d,
Minas M. Stylianakis^{a,e}, Lucy Di Silvio^d, Kiriaki Chrissopoulou^{a,*},
Spiros H. Anastasiadis^{a,b,**}

^a Institute of Electronic Structure and Laser, Foundation for Research and Technology - Hellas, 700 13, Heraklion, Crete, Greece

^b Department of Chemistry, University of Crete, 710 03, Heraklion, Crete, Greece

^c Department of Physics, University of Crete, 710 03, Heraklion, Crete, Greece

^d Faculty of Dentistry, Oral & Craniofacial Sciences, King's College London, London, SE19RT, United Kingdom

^e Department of Nursing, Hellenic Mediterranean University, 714 10, Heraklion, Crete, Greece

ARTICLE INFO

Keywords:

Superhydrophobic surfaces
Non-fluorinated molecules
Silicone-based nanocomposite coatings
Contact angle
Cytocompatibility

ABSTRACT

Fluorine-free superhydrophobic and water-repellent polymer nanocomposite coatings are developed on different substrates, like stainless steel, glass and polypropylene, utilizing a fluorine-free, silicone-based aqueous polymer emulsion (Protectosil® WS 610), to provide the appropriate hydrophobicity, and silica nanoparticles, to introduce the appropriate roughness; the coatings are prepared by a straightforward dip-coating process. The surface structure and topography of the resulting coatings were investigated using appropriate characterization techniques, while their wettability was evaluated with contact angle measurements. After thermal annealing of the polymer/silica nanocomposite films, the treated surfaces exhibited water contact angles exceeding 150° and very low contact angle hysteresis and roll-off angles, confirming their superhydrophobicity and water-repellence, respectively. Furthermore, the mechanical and chemical durability of the coatings was evaluated, revealing excellent stability under both highly acidic and highly alkaline conditions, as well as sustained performance during abrasion testing, while, more importantly, cytotoxicity testing confirmed the cytocompatibility of the coatings with the human skin. These findings demonstrate that Protectosil® WS 610/silica nanocomposites provide an effective and environmentally friendly route for developing fluorine-free superhydrophobic surfaces.

1. Introduction

Interest in the development of superhydrophobic surfaces has grown significantly during the recent years due to their wide range of potential applications [1–3]. Such surfaces can be utilized in self-cleaning materials [4–7], anti-fouling [8,9] and anti-icing coatings [10–12], stain-resistant textiles [13–15], fog-reducing surfaces [16–18], microfluidics [19,20], sensors [21,22], and drug delivery applications [23]. Superhydrophobic and water-repellent surfaces are characterized by very high water contact angles ($\geq 150^\circ$) and contact angle hysteresis less than $\sim 10^\circ$ that expresses the extremely low adhesion to water droplets. The development of such surfaces takes advantage of the combination of low surface energy materials and specific structural features on the

material surfaces that lead to hierarchical roughness [24–26]. Low surface energy is typically achieved via the use of very hydrophobic coating materials, while hierarchical roughness requires the surface to exhibit dual-scale roughness both at the micro- and nano-meter scale. The development of superhydrophobic and water-repellent surfaces is mimicking surfaces found in nature like certain plants and insects. One of the most famous plants, known for its very high contact angle in combination with its ultralow water adhesion, is the sacred Lotus leaf (*Nelumbo nucifera*) [27–29]. However, in many circumstances both in nature and in specific applications, superhydrophobic surfaces need to be accompanied by high water adhesion, where the water contact angle remains as high as 150° but the contact angle hysteresis is also large, resulting in a significant water droplet pinning on the surface [30–32].

This article is part of a special issue entitled: EPF-2025: Future Faculty published in Polymer.

* Corresponding author.

** Corresponding author. Institute of Electronic Structure and Laser, Foundation for Research and Technology - Hellas, 700 13, Heraklion, Crete, Greece

E-mail addresses: kiki@iesl.forth.gr (K. Chrissopoulou), spiros@iesl.forth.gr (S.H. Anastasiadis).

<https://doi.org/10.1016/j.polymer.2026.129851>

Received 24 January 2026; Received in revised form 11 March 2026; Accepted 12 March 2026

Available online 20 March 2026

0032-3861/© 2026 The Authors. Published by Elsevier Ltd. This is an open access article under the CC BY license (<http://creativecommons.org/licenses/by/4.0/>).

The development of superhydrophobic surface coatings involves the selection of suitable hydrophobic polymeric materials to achieve low surface energy, while the hierarchical roughness is attained using specific fabrication techniques. Various physical approaches, such as surface etching [33], lithography [34], laser texturing [4,35,36] and controlled crystal growth [3], are commonly employed to generate the hierarchical roughness required for superhydrophobic behavior, while chemical strategies (e.g., the application of hydrophobic agents or the incorporation of certain additives [37]) are used to tailor surface chemistry. Each of these methods allows different degree of control over topography and interfacial properties. Despite their higher cost, these techniques allow precise control over surface morphology, enabling the fabrication of surfaces with either random or periodic roughness patterns. However, their applicability is restricted to new material surfaces and not ones that are already in use. On the other hand, the utilization of polymer nanocomposites that incorporate (inorganic) nanoparticles added to a hydrophobic polymer matrix can itself create or amplify surface roughness [3]. When incorporated into polymer-based nanocomposite coatings and deposited on different substrates, ranging from metals and fibers to wood and stone [37–40], nanoparticles can significantly enhance water repellence and enable self-cleaning behavior. The selection of the nanoparticles largely depends on the specific application of the coated surface. For example, zinc oxide (ZnO) nanoparticles are commonly used due to their antibacterial properties and UV protection capabilities [41,42]. Similarly, titanium dioxide (TiO₂) nanoparticles exhibit comparable advantages, due to their photocatalytic properties [43]. Copper and silver nanoparticles provide antibacterial functionality and can contribute to surface roughness leading to superhydrophobicity [44,45]. Alumina Nanoparticles (Al₂O₃) have demonstrated water-repellent properties under hot water exposure, whereas silica nanoparticles (SiO₂) are frequently utilized in applications requiring high transparency, such as photovoltaic panels and greenhouse films [37,46,47]. In cases where water repellence is achieved through the application of a nanohybrid polymer coating, techniques such as dip-coating and spraying can be utilized even on large scales due to their simplicity, low cost and compatibility with industrial processes [48,49]. Depending on the processing conditions, i.e., temperature, solvent type, and solution concentration, these coating techniques can lead to the formation of thin polymeric films even on heterogeneous surfaces [50].

The development of superhydrophobic surfaces requires the use of hydrophobic materials with low surface energy, as well. Among the materials commonly used, fluorinated polymers are the most frequently employed, as their low surface energy when combined with hierarchical roughness can lead to water contact angles above 150°, enhancing water repellence [37,51–57]. The presence of fluorine atoms contributes significantly to the formation of highly hydrophobic surfaces due to the so-called fluorine effect that originates from the large size of fluorine, compared to hydrogen, resulting in an extreme version of the hydrophobic effect [58]. However, despite their excellent performance in enhancing hydrophobicity, fluorinated compounds have raised serious environmental and health concerns. Many of these compounds, particularly per- and polyfluoroalkyl substances (PFAS), are extremely persistent in the environment and resist natural degradation processes [59]. Toxicological studies have associated exposure to PFAS with a range of harmful effects, including endocrine disruption [60,61], carcinogenicity [62,63], water contamination [64–66], and ecotoxicity [67,68]. As a result, regulatory agencies are increasingly restricting or phasing out the use of certain fluorinated substances in industrial and consumer products [69]. Consequently, regulatory restrictions and growing environmental awareness have created an urgent need to develop sustainable, non-toxic, and eco-friendly alternatives.

Over the past decade, there has been some progress towards the development of fluorine-free superhydrophobic coatings, and few studies have demonstrated viable alternatives using green chemistries, biodegradable materials and simplified processing methods. The most commonly used polymers are silicone-based, such as poly(dimethyl

siloxane), PDMS, due to their enhanced hydrophobicity, which can contribute to the formation of superhydrophobic coatings [70]. For example, a PDMS-based coating fabricated via a phase-separation approach of a water/THF emulsion system has been reported [71] to induce superhydrophobicity and high transparency without the addition of nanoparticles; the surface roughness responsible for superhydrophobicity arises solely from the self-assembly and phase separation of the silicone polymer. PDMS has also been employed in the development of superhydrophobic coatings with enhanced durability utilizing SiO₂ or SiC/TiN nanoparticles and low-cost materials such as fly ash. These approaches often include two-step spraying methods followed by high-temperature curing to promote the crosslinking of the coatings [72,73]. The resulting surfaces can exhibit multifunctional properties, including self-cleaning, anti-icing and anti-corrosion behavior, making them suitable for a wide range of applications. Furthermore, silicone resins have been used in the fabrication of superhydrophobic, water-repellent and fire-resistant coatings. A multi-step formulation strategy was proposed, enabling deposition onto steel surfaces via a single-step spraying method. The coated surfaces possess mechanical durability, chemical stability and weather resistance [74,75]. A bilayer composed of silanes and silica colloids has also been developed and applied to floating solar cells; the resulting superhydrophobic coating exhibited antireflective, transparent, and self-cleaning properties, along with high mechanical durability [76]. Silane derivatives are also used in the textile industry for the development of superhydrophobic and water-repellent fabrics; if superhydrophobicity is combined with oleophilicity, the coated fabrics can also be used in oil-water separation applications [77,78]. Fabrics have also been modified with fluorine-free “superomniphobic” coatings, exhibiting excellent liquid repellence and long-term durability under harsh conditions [79]. Moreover, silane-based polymers have been combined with nanoparticles, such as CuO or TiO₂, for their antibacterial properties and photocatalytic activity, respectively [80,81]. Nonetheless, there are studies that have highlighted the use of different polymers for the development of superhydrophobic coatings [82] as well, with an emphasis on more bio-based and sustainable materials [83].

In the present work, we introduce a simple, eco-friendly, and nanoparticle-based approach for the development of fluorine-free superhydrophobic coatings utilizing a new commercial siloxane-based waterborne emulsion and silica nanoparticles, which enables the fabrication of high-performance coatings through a straightforward dip-coating process. The developed nanohybrid polymer coating exhibits highly water-repellent and superhydrophobic behavior, while remaining safe for potential human contact. In addition, the coating was successfully applied to a wide range of commonly used substrates, such as stainless steel, glass and polymer, demonstrating its broad versatility, while the cytotoxicity testing confirmed the cytocompatibility of the coatings with the human skin. This method is simple, low-cost, and scalable, and was specifically designed to avoid the use of fluorinated derivatives, making it a practical and environmentally responsible solution for functional surface modification. Moreover, all coated surfaces exhibit remarkable durability in harsh acidic and alkaline conditions, however further investigations on the enhancement of the mechanical durability are needed.

2. Experimental

2.1. Materials

Protectosil® WS 610, provided by Evonik, is a low surface energy material that is utilized in the current work for the development of superhydrophobic coatings. It is a non-fluorinated, organofunctional, waterborne emulsion consisting of silanes and siloxanes, and it is free of volatile organic compounds (VOCs). In its commercial form, the Protectosil® emulsion is white in appearance, it has a solid content of

approximately 50 wt% and a pH value of about 8.5. Protectosil® is a film forming material and, according to the manufacturer, when deposited on a surface under high pH conditions, the emulsion particles break apart and hydrolysis occurs, leading to the formation of -SiOH groups. These groups subsequently undergo condensation either with each other or with -OH groups present on the substrate, forming a siloxane network that is covalently bonded to the coated surface. It is noted that prior to its use, the dispersion was diluted with distilled water until it reached concentration 4 wt%.

Protectosil® WS 610 was characterized using dynamic light scattering (DLS) at a concentration of 0.06 wt%, to assess the size distribution of the emulsion particles dispersed in water. The results indicate that the particles possess a hydrodynamic diameter of 328 ± 6 nm (Fig. S1a of the Supplementary Data). The chemical structure of the material was further investigated by infrared spectroscopy (ATR-FTIR). The IR spectrum (Fig. S2) revealed characteristic absorption bands indicative of a silicon-based polymeric structure. These characteristic bands that denote the presence of siloxane (Si-O-Si), silanol (Si-OH) and organosilicon (Si-C) bonds are reported in Table S1. Peaks associated with organic groups such as C-H and C=C were also observed, while a broad O-H stretching band likely results from moisture absorption [84–87].

Silicon dioxide (SiO₂) nanoparticles are utilized for the development of the nanohybrid coatings. The nanoparticles were purchased from Nanochemazone in an aqueous dispersion, with an initial concentration of 0.7 wt%. Particle size analysis via Zetasizer indicated a mean diameter of 162 ± 9 nm, while the dispersion exhibited a pH of 8.5.

Coatings with different inorganic content were prepared via a simple mixing of the diluted dispersion of Protectosil® with nanoparticle dispersions of varying concentrations. Dipping was selected as the deposition method employed for the development of both the neat polymer and the hybrid coatings. Substrates were immersed vertically into the dispersion for 20 s; they were, then, removed and they were placed under vacuum overnight to dry and ensure proper film formation. In cases where annealing was performed, the coated surfaces were subjected to annealing under vacuum conditions at 65 °C for a duration of 24 h.

Three different types of substrates were used for the evaluation of the coatings: stainless steel AISI 304 plates obtained by ARST (water contact angle, WCA = $46 \pm 2^\circ$), homopolymer polypropylene sheets purchased from Goodfellow (WCA = $90 \pm 2^\circ$) and glass microscope slides from Labbox (WCA = $35 \pm 2^\circ$), each with dimensions of 1 cm × 1 cm. Due to their inherent hydrophobicity, the polypropylene substrates required an additional plasma treatment prior to the coating deposition; this step was necessary to increase the surface energy of the polymer substrates and to introduce functional groups that promote improved adhesion of the applied coatings. The plasma treatment was performed using the PiezoBrush® PZ3 device (Relyon Plasma GmbH). Before treatment, all substrates were thoroughly cleaned sequentially with distilled water and ethanol.

2.2. Experimental techniques

2.2.1. Contact angle measurements

The wetting behavior of the coated surfaces was evaluated using an OCA-35 contact angle measuring device from Dataphysics, with SCA-20 software. The contact angle measurements were performed using the sessile drop method (static contact angle). Water droplets (4 µL) were deposited onto the surface at a controlled deposition rate of 1 µL/s, using a Hamilton 500 µL microsyringe. All experiments were carried out under ambient temperature and pressure conditions. To evaluate the contact angle hysteresis, the tilting method was employed: the substrate is tilted between 0° and 90° at a constant rate of 1° s^{-1} , whereas drop volumes between 4 µL and 30 µL are used to simulate different water droplet sizes. The advancing and receding angles are measured just before the drop begins to move on the tilted substrate, whereas the angle at which

the drop moves provides the roll off angle of the surface for the particular drop volume.

2.2.2. Scanning Electron Microscopy (SEM)

The surface morphology of the samples was imaged using a JEOL JSM-6390VL Field Emission Scanning Electron Microscope (FE-SEM). The coated substrates were mounted on a glass surface using carbon tape and were coated with a 15.6 nm layer of gold via sputtering to ensure conductivity. The instrument operated with an accelerating voltage of 15 kV, and the magnification of the samples images was ranging between $\times 5$ to $\times 300,000$. The microscope was equipped with an integrated Energy Dispersive X-ray Spectrometer (EDS) for chemical and elemental analysis.

2.2.3. Atomic Force Microscopy (AFM)

Surface roughness was evaluated using a Bruker Dimension ICON AFM equipped with a Controller VI. Measurements were conducted over an area of $80 \times 80 \mu\text{m}^2$ with a resolution of 512 points per line and a scan rate of 0.996 Hz. The measurements were carried out at a drive frequency of 343 kHz and a drive amplitude of 101.6 mV, ensuring accurate characterization of the surface topography.

2.2.4. Profilometry

The coating thickness was determined by surface profilometry using a Veeco Dektak 150 profilometer. The instrument employed a 12.5 µm radius stylus that scanned the sample over a length of 800 µm. The scan duration was 60 s, ensuring detailed surface analysis. A contact force of 4.0 mN was applied by the stylus, which is considered sufficient for accurate measurements without damaging the surface. The average coating thickness and the corresponding standard deviation was obtained from measurements at various locations of the surface for each coating as well as for different coated surfaces.

2.2.5. Cytocompatibility protocol

Cytocompatibility was measured in line with ISO 10993-5 (Tests for in vitro cytotoxicity), which states that materials are considered cytotoxic when cell viability falls below 70% compared to a negative control. Prior to testing, all coated surfaces were sterilized under UV light. Human dermal fibroblasts (HDF1, passage 9) were used as the cellular model. Cells were cultured in Dulbecco's Modified Eagle Medium (DMEM), enriched with 10% v/v fetal calf serum (FCS), 1% v/v penicillin/streptomycin and 1% v/v glutamine. After a 24 h incubation at 37 °C in a 5% v/v CO₂ atmosphere, HDF1 cells were washed with PBS, after which the coated and uncoated stainless steel samples were placed in direct contact with the apical cell surface; these constituted the experimental group. Untreated HDF1 cells served as the negative control and were designated as the BLANK group. After 1 h, the samples were removed and the cells in all groups were washed once with PBS and the medium was replaced with serum-free DMEM. Cells were then incubated for an additional 24 h prior to viability assessment, using WST-8 and Alamar Blue cytotoxicity assays, which are based on metabolic activity. A 20% v/v DMSO solution served as positive control.

2.2.6. Abrasion Tests

Abrasion tests were carried out to investigate the scratch resistance of the coatings using the sandpaper-based method. For the abradant surface, 2000 grit aluminum oxide sandpaper was used. Each coated sample was pressed face-down against the sandpaper under a 100 g load and moved over a distance of 10 cm. This operation was defined as one abrasion cycle and each of the investigated surfaces underwent 40 cycles.

Abrasion test measurements were also performed using an Elcometer 1720 Abrasion and Washability Tester, utilizing a microfiber coated tool, a load of 420 g and a speed of 25 cycles.min⁻¹ for multiple abrasion cycles.

3. Results and discussion

3.1. Polymer coatings

Polymer coatings were developed on different substrates by dipping, and their surface topology was examined. Fig. 1a shows a SEM micrograph of the deposited polymer on stainless steel, indicating the presence of discrete particles rather than a continuous film. Therefore, a “simple” deposition of the polymer using dipping is insufficient for an effective film formation. Although the particles observed on the surface in the SEM image appear larger (a few μm), than those measured by DLS (~ 300 nm), this difference arises from the fact that DLS reflects the hydrodynamic size of dispersed particles in solution, whereas SEM captures their morphology after deposition and drying. During this process, partial coalescence or spreading of the polymer particles can occur, leading to the larger surface features observed in the coating.

According to the polymer emulsion provider, the formation of a homogeneous film requires the particles of the Protectosil® emulsion to be broken, which is accomplished under high-pH conditions. To evaluate the most effective way to do this, both the direct addition of an alkaline solution to the polymeric dispersion prior to coating and a post-deposition spraying of the coated surface with the same alkaline aqueous solution were tested.

In the first approach, sodium hydroxide (NaOH, 0.1 M) was added dropwise to the polymer dispersion to adjust the pH to 9 or 12 prior to coating. DLS measurements for the pH adjusted dispersions showed no change in the particle size, with the hydrodynamic diameter remaining constant at 330 ± 6 nm (Fig. S1b). This indicates that the polymer particles are stable under alkaline conditions, and adjusting the pH of the dispersions does not promote the breakdown of the polymer particles required for film formation. Moreover, in both cases, (i.e., deposition from the original and from the pH-adjusted dispersions), the dipping procedure did not result in the formation of a homogeneous film. Water contact angles were measured on the coatings prepared by dipping in the original suspensions and in the ones after pH-adjustment

of the emulsion as a function of time after deposition. The initial static water contact angle for all coatings prepared from 4 wt% Protectosil® dispersions on stainless steel substrates was approximately 60° , as shown in Fig. S3. A gradual increase in water contact angle was observed during the first week after preparation, which reached 90° – 100° after one week and remained constant over the following weeks. This behavior indicates that film formation and surface reorganization primarily occur within the first week, leading to a stable hydrophobic state. Therefore, this method, although eventually producing hydrophobic coatings, is not suitable for rapid and practical film formation.

In the second approach, polymeric coatings were first deposited on stainless steel, polypropylene (after plasma treatment), and glass substrates by dip-coating into aqueous Protectosil® dispersions at concentrations ranging from 1 wt% to 50 wt%. The coated samples were vacuum-dried at ambient temperature overnight to remove residual water. As a post-deposition treatment, the dried coatings were sprayed 2–3 times with a 0.1 M NaOH solution (pH = 9), followed by a second drying step.

SEM analysis of the coated surfaces confirmed the effectiveness of this method. Fig. 1b illustrates the topography of a coated stainless steel surface after deposition from a Protectosil® WS 610 dispersion of 4 wt%, which was subsequently sprayed with high-pH solution; a smooth, continuous film morphology is observed in contrast to the discrete emulsion particles observed before treatment (see Fig. 1a). The absence of emulsion particles in the SEM images indicates that the alkaline spray method effectively leads to the breaking of the emulsion particles, enabling the formation of a well-developed, crosslinked, silicone-based coating. This process likely promotes the generation of silanol groups via hydrolysis, followed by their subsequent condensation. Elemental mapping for the sprayed coating was subsequently conducted and the C, O and Si distribution maps shown in Fig. 1c–e illustrate the presence of all three elements, which homogeneously cover the whole surface, proving thereby the compositional homogeneity of the coating. Complementing these observations, Table S2 shows the corresponding EDS quantification for the sprayed coating, confirming the presence and the

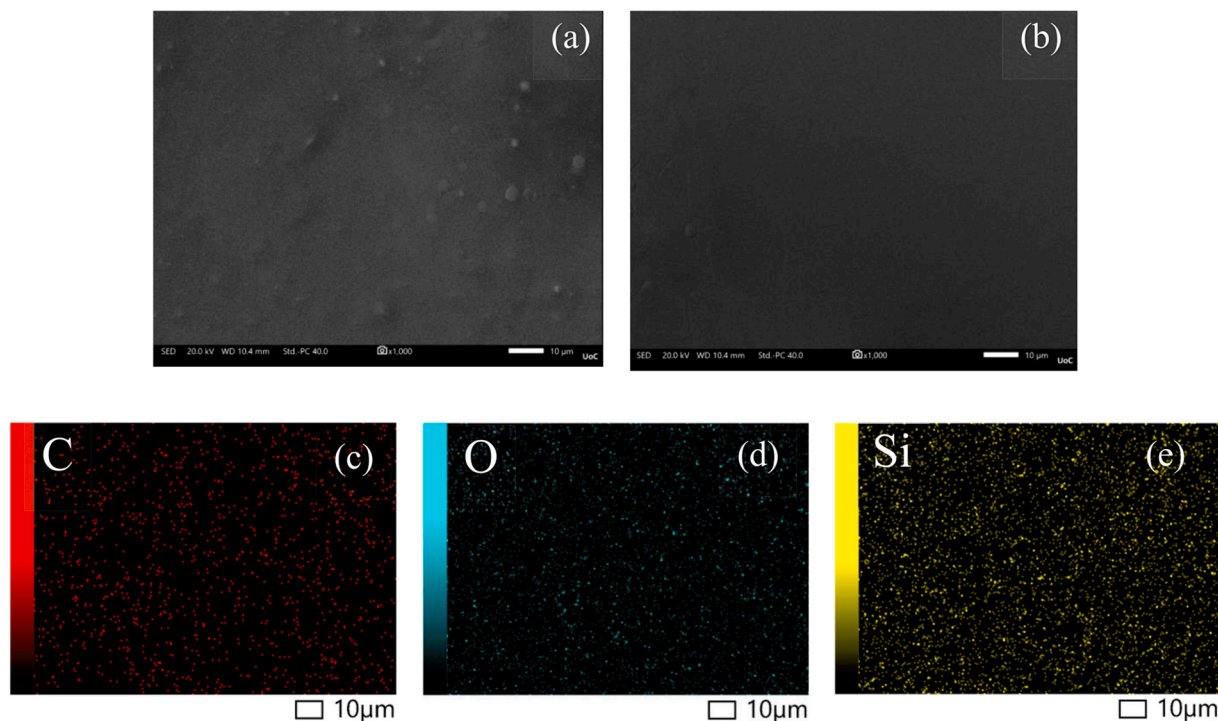


Fig. 1. SEM images of Protectosil® WS 610 on stainless steel substrate at a magnification of $\times 1000$ (the scale bar corresponds to 10 μm) following (a) “simple” dipping deposition. (b) after spraying the coating with a high-pH solution. (c–e) Elemental mapping images for C, O and Si (from left to right) of the sprayed coating. The scale bar corresponds to 10 μm .

respective ratios of each element in the above mapping analysis.

To evaluate the surface roughness and thickness of the polymer coatings, AFM and profilometry measurements were conducted, respectively. Fig. 2 presents AFM topographical images of stainless steel substrates coated with Protectosil® after dipping in a 4 wt% dispersion, before (Fig. 2, top row) and after (Fig. 2, bottom row) the alkaline spraying step. In Fig. 2-top, the surface prior to spraying shows distinct emulsion particles and pronounced roughness. After treatment with the high-pH aqueous solution (Fig. 2-bottom), the surface becomes significantly smoother, exhibiting an RMS roughness of 7.5 nm. This reduction confirms the breakup of the emulsion particles and the formation of a more homogeneous, continuous silicone-based resin layer. These findings further support the evidence from SEM and contact angle measurements regarding particle rupture and resin network development. Moreover, coatings prepared on stainless steel via dipping in a 4 wt% dispersion followed by spraying with a high-pH aqueous solution exhibited a uniform thickness with a mean value of $0.75 \pm 0.06 \mu\text{m}$, as determined by profilometry (indicative scan shown in Fig. S4).

Fig. 3 shows equilibrium water contact angles for Protectosil® WS 610 coatings of different thicknesses (corresponding to the dispersion concentration) onto stainless steel, polypropylene, and glass substrates after post-deposition spraying with high-pH aqueous solution. For stainless steel and glass, the contact angles increased substantially, reaching approximately 100° at concentrations up to 25 wt% and, then, decreased for concentrations up to 50 wt%, likely due to incomplete reaching of the emulsion particles by the spraying solution, leaving some particles partially untreated or aggregated. In contrast, coatings deposited on polypropylene exhibited consistently high contact angles of $\sim 100^\circ$ across all concentrations, which is attributed to the plasma treatment applied to polypropylene prior to coating. This pre-treatment facilitates breakup of the particles in the coating enhancing surface

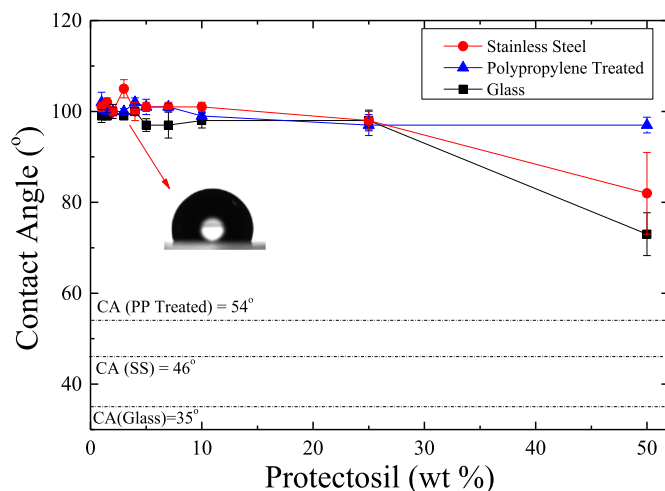


Fig. 3. Equilibrium water contact angles for Protectosil® WS 610-coated stainless steel, polypropylene and glass substrates as a function of Protectosil® WS 610 concentration in aqueous dispersions, after spraying with an alkaline aqueous solution (pH ~ 9). The dotted lines indicate the water contact angles on each of the different substrates without a coating.

hydrophobicity. These findings demonstrate that the high-pH spraying method is most effective within an optimal concentration range; for the rest of the work a 4 wt% dispersion concentration was utilized since it was providing a homogeneous film and a high water contact angle value.

The polymer coatings deposited on stainless steel substrates after spraying with an alkaline aqueous solution were further examined in terms of their contact angle hysteresis and roll-off angles of water

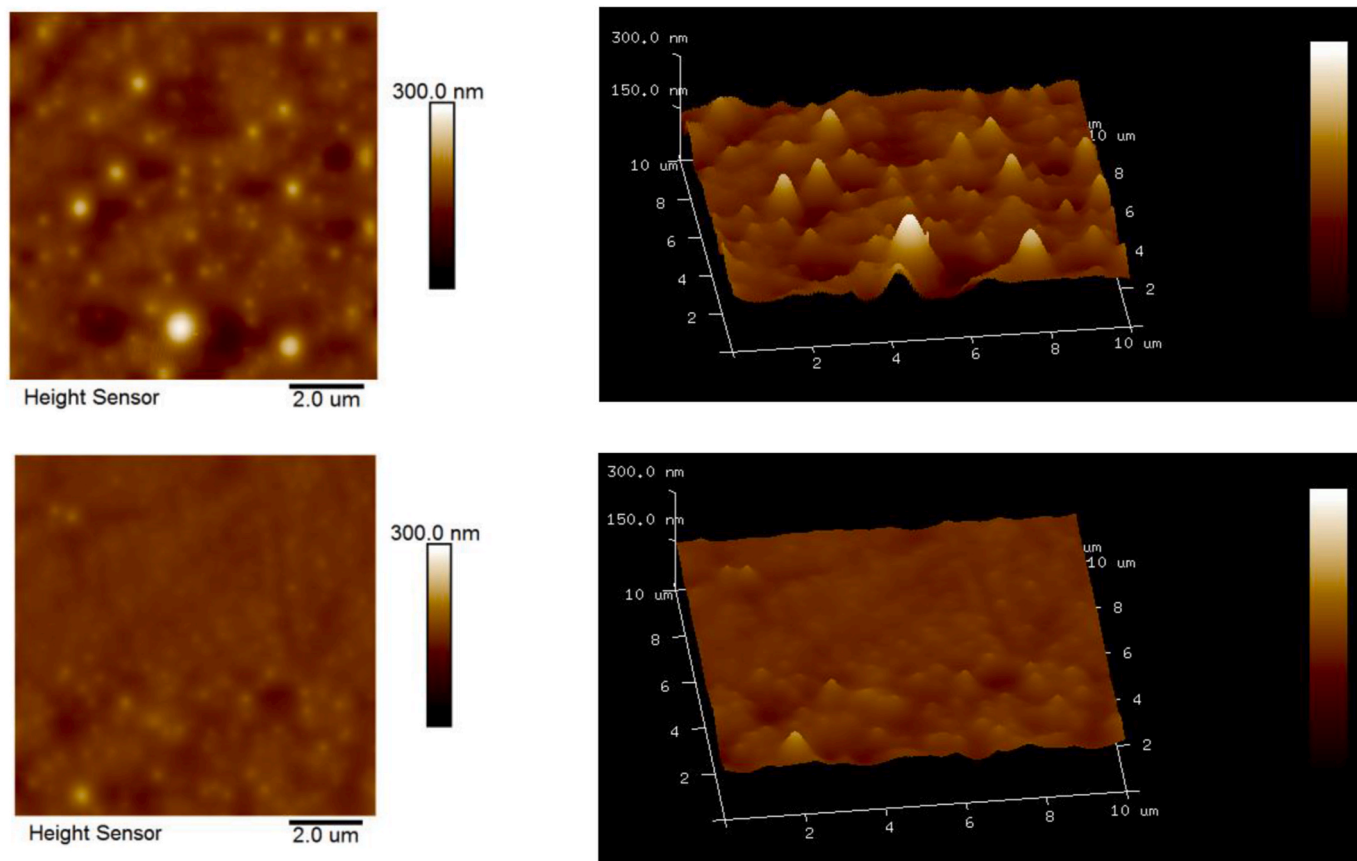


Fig. 2. AFM micrographs of Protectosil® coatings on stainless steel: (top row) before and (bottom row) after spraying with a high-pH aqueous solution. The scale bar in the x-y axis is $2 \mu\text{m}$ and in the z-axis 300 nm .

droplets. Table 1 presents the results for different volumes of the water droplets (4, 10, 20, and 30 μL). A decrease in the values of the roll off angle is observed, which ranges from 32° for a droplet of 4 μL volume to 14° for a droplet of 30 μL . It should be noted that even the smallest droplet exhibited roll-off behavior, indicating a low-adhesion surface even though the surface is only weakly hydrophobic. At the same time, contact angle hysteresis values remained consistently low, in the range of $\sim 10^\circ$, further confirming the high-quality hydrophobic performance of the sprayed Protectosil® coatings. These results indicate a hydrophobic surface exhibiting pronounced water repellence and relatively low contact angle hysteresis.

Moreover, viability assessments were carried out for Protectosil® coatings on stainless steel to evaluate the cytocompatibility of the developed materials. According to ISO 10993-5, a reduction in cell viability to below 70% of the negative control indicates cytotoxic potential. Stainless steel surfaces uncoated and coated with 4 wt% aqueous Protectosil® dispersions were evaluated using both WST-8 (Water-Soluble Tatzazoliun 8) and Alamar Blue assays, and the results are shown in Fig. 4.

In the experimental and control groups, cell viability was maintained well above the viability threshold, with WST-8 measurements yielding $79.9\% \pm 7.1\%$ and Alamar Blue results reaching $99.8\% \pm 2.1\%$. These findings confirm that these polymer coatings are safe for potential applications involving direct contact with human cells and further support their safe utilization.

3.2. Nanohybrid coatings utilizing SiO_2 nanoparticles

Polymer nanocomposite formulations were subsequently utilized to further enhance the surface properties of the resulting coatings. These formulations were prepared by mixing an aqueous 4 wt% Protectosil® dispersion with aqueous dispersions of SiO_2 nanoparticles at various concentrations, aiming to achieve an inorganic content between 10 and 50 wt% in the final coatings. The nanocomposite dispersions were utilized to develop nanohybrid coatings onto stainless steel, PP and glass substrates by dipping, and, in all cases, the coatings were subsequently sprayed with a high-pH aqueous solution as well.

Fig. 5 shows the values of static water contact angles as a function of silica nanoparticle content in the nanohybrid coatings that have been deposited on stainless steel by dipping. Data are shown for measurements on the as-prepared coatings and on coatings after the spraying with the high-pH aqueous solution. It is evident that prior to spraying, the addition of SiO_2 leads to a gradual increase of the contact angles, which stabilize above 120° for nanoparticle contents ≥ 30 wt%. This trend indicates that the incorporation of silica enhances surface roughness, thus promoting the apparent hydrophobicity. For the coatings with 10 wt% SiO_2 content, the contact angle values show a significant increase following the spraying step, with a difference of approximately 30° compared to the coating that has not undergone spraying with the high-pH solution. However, when the nanoparticle loading reaches or exceeds 20 wt%, the contact angles remain essentially unchanged before and after spraying, suggesting that such silica concentrations are sufficient to induce the breakdown of the emulsion particles, without the

Table 1

Advancing and receding contact angles and roll-off angles for water droplets of varying volumes for Protectosil® coatings on stainless steel, after spraying with an alkaline aqueous solution. The mean static water contact angles for drop volumes of 4–30 μL , are $\theta_0 = 99^\circ \pm 3^\circ$.

Water Droplet Volume (μL)	Protectosil® Coatings on Stainless Steel		
	Roll off Angle ($\pm 1^\circ$)	θ_{adv} ($\pm 3^\circ$)	θ_{rec} ($\pm 3^\circ$)
4	32°	99°	91°
10	21°	100°	92°
20	17°	94°	81°
30	14°	97°	84°

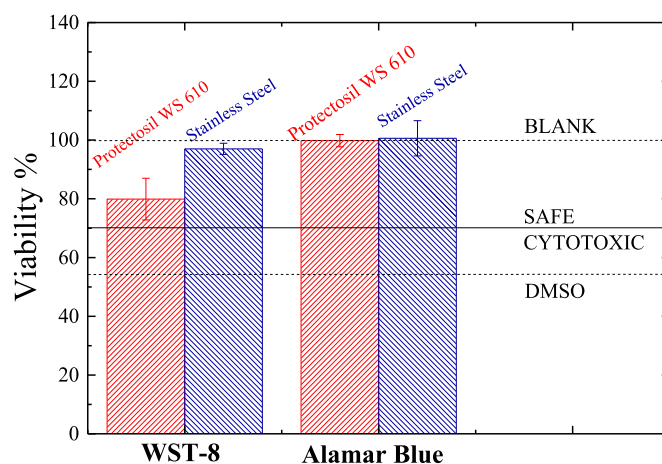


Fig. 4. Viability assessment of coatings deposited from a 4 wt% Protectosil® dispersion on stainless steel substrates evaluated using (a) WST-8 and (b) Alamar Blue assays. Results for uncoated stainless steel substrates are included for comparison. Cells not exposed to stainless steel surfaces served as the negative control and were designated as the BLANK group. Cells treated with 20% DMSO served as the positive control, confirming assay sensitivity to cell death.

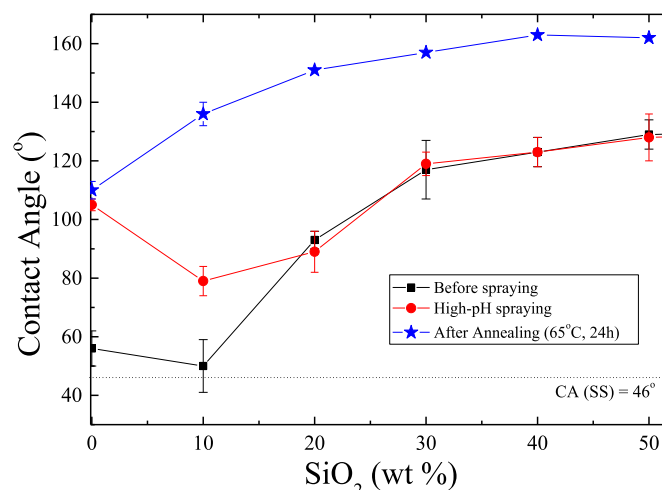


Fig. 5. Water contact angle values for droplets on stainless steel substrates coated with Protectosil®/ SiO_2 nanoparticles formulations with varying inorganic content. Data are shown for the as prepared coatings before spraying (black squares), coatings after spraying with high-pH aqueous solution (red circles) and coatings following spraying and thermal annealing at 65°C for 24 h (blue stars). The dotted line indicates the water contact angle for neat stainless steel. (For interpretation of the references to colour in this figure legend, the reader is referred to the Web version of this article.)

need for high-pH spraying. It is worth noting that the SiO_2 dispersions themselves exhibit a relatively high pH (~ 8.5). Consequently, for silica content ≥ 20 wt%, post-deposition spraying is not required. It is noted that similar results have been obtained in the case of polypropylene and glass substrates, as shown in Fig. S5 of the Supplementary Data. These findings highlight the significant role of the silica nanoparticle addition, both in the formation of a homogeneous coating and in controlling the topography and wettability of the coated surface.

It is evident that the incorporation of silica nanoparticles into the coating increases the water contact angle, which reaches values of 120° for coatings containing 50 wt% SiO_2 , therefore increasing the apparent hydrophobicity by increasing surface roughness. Nevertheless, advancing - receding contact angles and roll off angle measurements revealed that the nanohybrid coatings exhibit poor water repellence, performing even worse than the neat polymeric coating. More

specifically, Table 2 summarizes the advancing and receding contact angles as well as the roll-off angles measured after spraying the different nanocomposite coatings. Roll-off measurements were conducted with water droplets from 4 to 30 μL but only the 30 μL droplets rolled off (the corresponding images are provided in Table S3), at a tilt angle of about 50° for the formulations containing 30 wt% and 40 wt% SiO_2 . Increasing the inorganic content to 50 wt% improved slightly the water-repellent behavior since roll-off occurred at a lower angle of about 43° . However, in all cases the contact angle hysteresis values remained high, when compared to the corresponding ones of the neat polymeric coating; the latter exhibited roll-off angles ranging between 32° and 14° depending on the droplet size and contact angle hysteresis $\sim 10^\circ$ (see Table 1). Therefore, although the incorporation of SiO_2 increased the static contact angle, it also substantially enhanced water droplet adhesion, suggesting that, although the presence of the nanoparticles increases the surface roughness, this roughness is heterogeneous and, thus, the nanoparticles likely act as pinning sites on the surface rather than promoting easy droplet motion.

Thermal annealing of the nanocomposite coatings was subsequently performed to assist the formation of a more homogeneous roughness. The nanocomposite coatings, which were sprayed with high-pH aqueous solutions, were annealed at 65°C for 24 h under vacuum. It is noted that this temperature was chosen since it was the lowest temperature that resulted in superhydrophobic coatings following annealing. Contact angle measurements were performed on the annealed coatings and the results are shown in Fig. 5, as well. It is evident that annealing leads to a remarkable increase in the measured contact angle values, even at low SiO_2 concentrations. More specifically, even for coatings with 10 wt% nanoparticle content, the values of the water contact angles increase by more than 60° , approaching 140° , whereas, for concentrations between 20 wt% and 50 wt%, the surface becomes gradually superhydrophobic, reaching values up to 160° . Moreover, the surfaces have become water-repellent as well. Fig. 6 illustrates snapshots of the dynamic interaction between a water droplet (13 μL volume) and a nanocomposite coating containing 30 wt% SiO_2 nanoparticles after thermal annealing, which is tilted at 5° . Upon impact, the droplet bounces off the surface without wetting or adhering to it, demonstrating highly water-repellent behavior with extremely low contact angle hysteresis, which is less than 5° (Video S1 in the Supplementary Data). This water repellence ability of the coating results in self-cleaning properties of the surface as shown in Video S2 of the Supplementary Data for a such coated surface that has been polluted with dirt particles.

Similar bouncing was observed for all coatings with ≥ 20 wt% SiO_2 nanoparticle content, confirming the transition to a water-repellent state. In contrast, the coating with 10 wt% SiO_2 , although it exhibited a relatively high static contact angle ($\sim 140^\circ$), it did not show water repellence.

The remarkable change in the contact angle and the contact angle hysteresis behavior of the coated surfaces is likely because of the effect of thermal annealing on the homogeneity of the coatings. This is supported by the SEM micrographs of the nanocomposite coatings with 30 wt% SiO_2 , presented in Fig. 7a,b, at magnification of $\times 5000$. Fig. 7a shows that, before thermal annealing, the surface exhibits significant heterogeneity with many irregularities, indicative of non-uniform particle distribution. In contrast, the coatings after annealing (Fig. 7b) reveal a much more “homogeneously rough” morphology with consistent roughness patterns across the surface. Apparently, the thermal

treatment provides the energy required for the particles to reorganize themselves within the coating, leading to a more uniform particle distribution and a homogeneous hierarchical surface roughness. This apparent rearrangement of relatively large particles (hydrodynamic diameter of 160 nm) contributes to the observed increase in water contact angles and the enhanced water-repellent behavior.

Elemental mapping was performed for both before and after thermally annealed surfaces, at an identical magnification of $\times 5000$, to investigate the elemental distribution on the surface. The mapping reveals that the O and Si signals are significantly more intense in the nanocomposite compared to the polymeric coating (see Fig. 1c–e), which is attributed to the presence of the silica nanoparticles. The comparison between Fig. 7c and d indicates that the carbon signal does not change noticeably between the non-annealed and the annealed cases. Oxygen and silicon are present on the surface before annealing (Fig. 7e and g), though clear gaps and discontinuities in the signals are observed, similar to the heterogeneity of the surface seen in the SEM images. However, after thermal annealing, the signals of these two elements become stronger and the surface looks fully covered without gaps (Fig. 7f and h). This means that there is homogeneity in the inorganic phase distribution caused by rearrangement of the particles upon thermal treatment. Additional SEM images at magnifications of $\times 1000$, $\times 5000$, and $\times 10,000$ before and after annealing are shown in Fig. S6, where the differences can be more clearly observed.

In addition to the SEM observations, AFM measurements were performed before and after annealing. As shown in Fig. 8, the surface roughness significantly decreases after annealing, which is attributed to nanoparticle rearrangement. Specifically, before annealing, the RMS roughness is 628 ± 30 nm, while, after annealing, the value decreased to 179 ± 30 nm, indicating a smoother and more uniform surface.

Moreover, EDS analysis showed that the increased Si and O signals are accompanied by decreased chromium (Cr) and iron (Fe) signals from the substrate after annealing, indicating improved nanoparticle dispersion and more uniform coating coverage (Table S4). This is attributed to the thermally induced rearrangement of the silica nanoparticles, improving the surface coverage. Hence, the EDS detector becomes less sensitive to the elements constituting the substrate and, as a consequence, the relative percentages of Si and O in the spectrum increase.

Finally, cytocompatibility assessments of the nanocomposite coatings containing SiO_2 were conducted before (Fig. 9a) and after (Fig. 9b) thermal annealing. Prior to annealing, the WST-8 assay showed a viability of $84.4\% \pm 8.8\%$ and the Alamar Blue assay $95.2\% \pm 6.5\%$, indicating improved cytocompatibility compared to neat polymer coatings (Fig. 4). After annealing, viability further increased to $88.6\% \pm 1.5\%$ (WST-8) and $102.1\% \pm 3.8\%$ (Alamar Blue), demonstrating excellent cytocompatibility. These favorable results suggest that the coatings are safe and suitable for potential applications on high-touch surfaces.

3.3. Mechanical and chemical durability

The mechanical durability of the coatings was determined by performing abrasion tests using the sandpaper method. Fig. 10 shows water contact angle values following several abrasion cycles for Protectosil® coatings (black squares), these possess an initial value of $105^\circ \pm 2^\circ$, and undergo a slight reduction reaching $98^\circ \pm 2^\circ$, after 40 abrasion cycles. This slight decrease indicates that the Protectosil® film is not especially

Table 2

Advancing and receding contact angles and roll-off angles for 30 μL water droplets for hydrophobic nanocomposite coatings with Protectosil® WS 610 and SiO_2 nanoparticles on stainless steel, after spraying with high-pH aqueous solution. θ_0 is the equilibrium water contact angle.

Water Droplet Volume (μL)	30 wt% SiO_2 ($\theta_0 = 119^\circ \pm 4^\circ$)			40 wt% SiO_2 ($\theta_0 = 123^\circ \pm 5^\circ$)			50 wt% SiO_2 ($\theta_0 = 128^\circ \pm 8^\circ$)		
	Roll off Angle ($\pm 1^\circ$)	θ_{adv} ($\pm 1^\circ$)	θ_{rec} ($\pm 1^\circ$)	Roll off Angle ($\pm 1^\circ$)	θ_{adv} ($\pm 1^\circ$)	θ_{rec} ($\pm 1^\circ$)	Roll off Angle ($\pm 1^\circ$)	θ_{adv} ($\pm 1^\circ$)	θ_{rec} ($\pm 1^\circ$)
30	50°	120°	71°	52°	137°	69°	43°	117°	61°

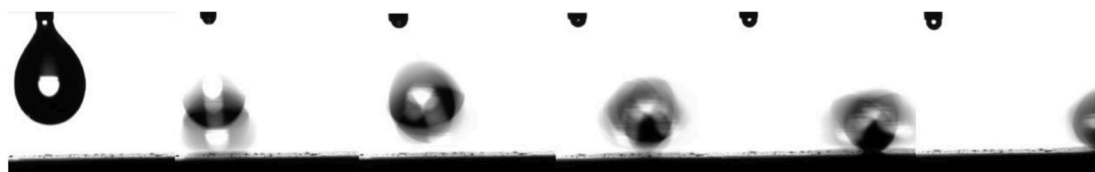


Fig. 6. Illustration of the water repellence of a stainless steel substrate coated with a nanocomposite coating containing 70 wt% Protectosil® WS 610 and 30 wt% SiO₂ nanoparticles, following annealing at 65 °C for 24 h. The water droplet volume is 13 µL and the substrate is tilted by 5°.

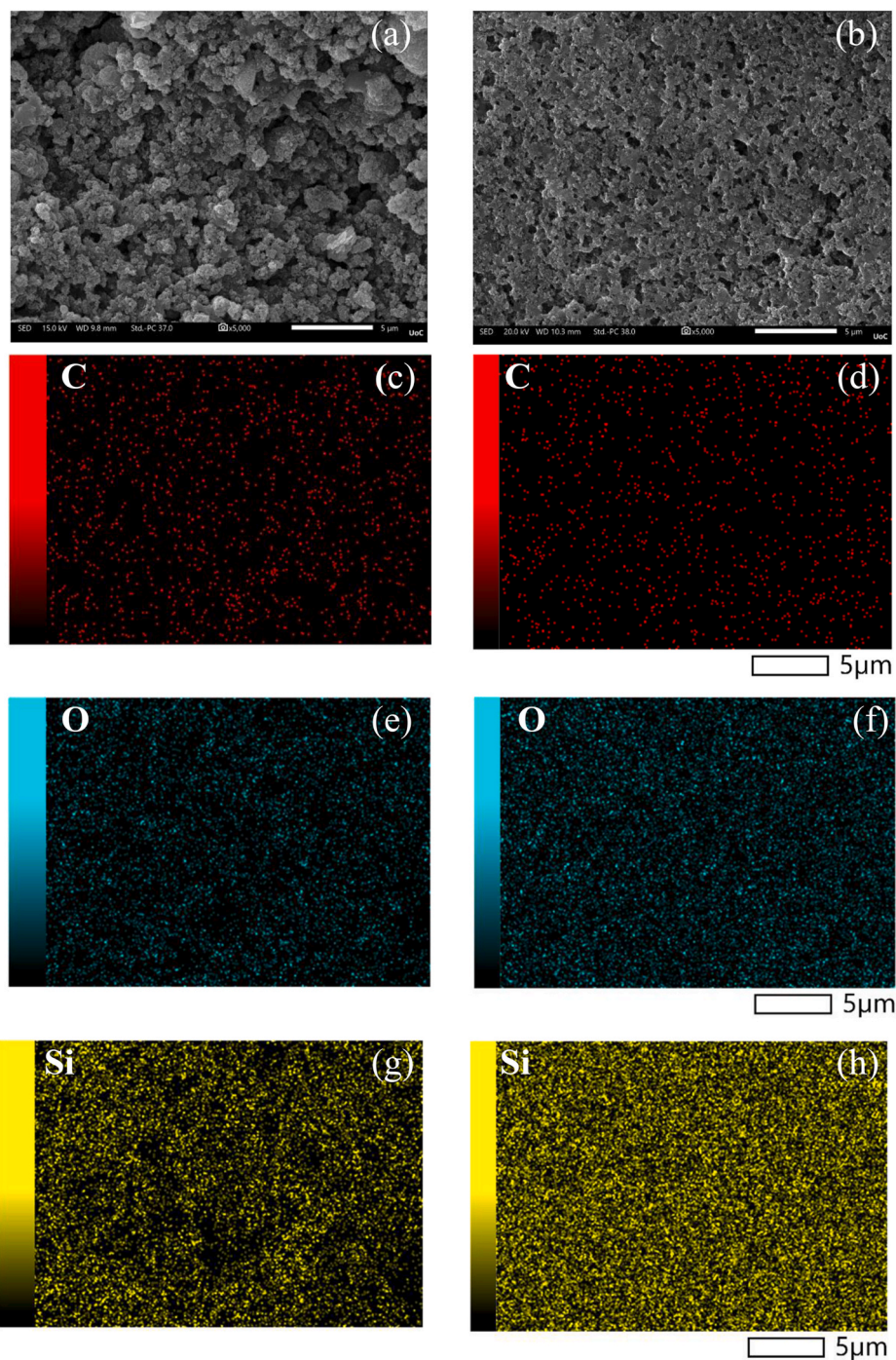


Fig. 7. SEM images before (a) and after (b) thermal annealing at 65 °C for 24 h for the Protectosil® WS 610 coating on stainless steel containing 30 wt% SiO₂ nanoparticles, at magnifications of $\times 5000$. The scale bars correspond to 5 µm. Elemental mapping of carbon (C), oxygen (O) and silicon (Si) at a magnification of $\times 5000$, shown before (c,e,g) and after (d, f, h) thermal annealing. The scale bar corresponds to 5 µm.

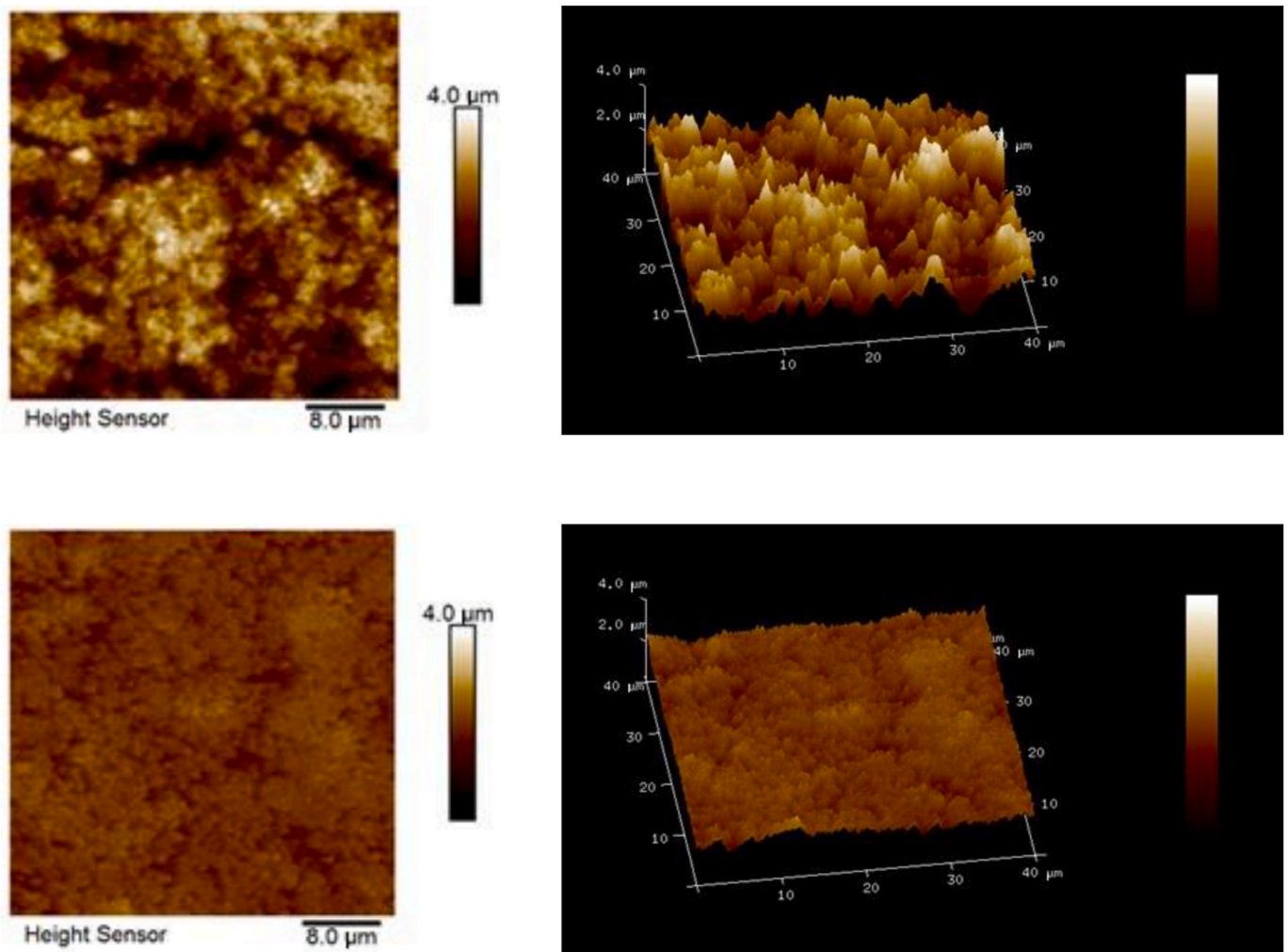


Fig. 8. AFM images of the 70 wt% Protectosil® WS 610 and 30 wt% SiO₂ nanoparticles coating on stainless steel before (top row) and after (bottom row) annealing at 65 °C for 24 h. The scale bar in the x-y axis is 8 μm and in the z-axis is 4 μm.

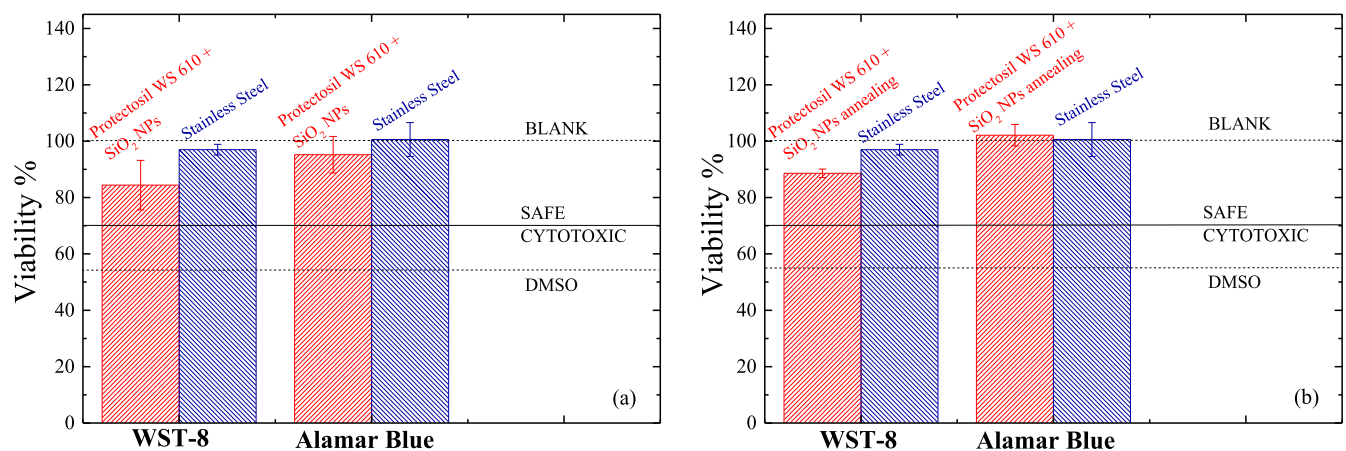


Fig. 9. Viability tests evaluated using WST-8 and Alamar Blue assays for 70 wt% Protectosil® WS 610 + 30 wt% SiO₂ coatings on stainless steel substrates (a) before and (b) after annealing. Results for uncoated stainless steel substrates are included for comparison. Cells not exposed to stainless steel surfaces served as the negative control and were designated as the BLANK group. Cells treated with 20% DMSO served as the positive control, confirming assay sensitivity to cell death.

affected by mechanical wear and indicates good adhesion of the polymer onto the stainless-steel surface.

In contrast, coatings containing Protectosil® with 30 wt% SiO₂

nanoparticles display distinctly different behavior. Indeed, the coatings exhibit high contact angles during the first few cycles both before and after thermal annealing, maintaining strong hydrophobicity. However,

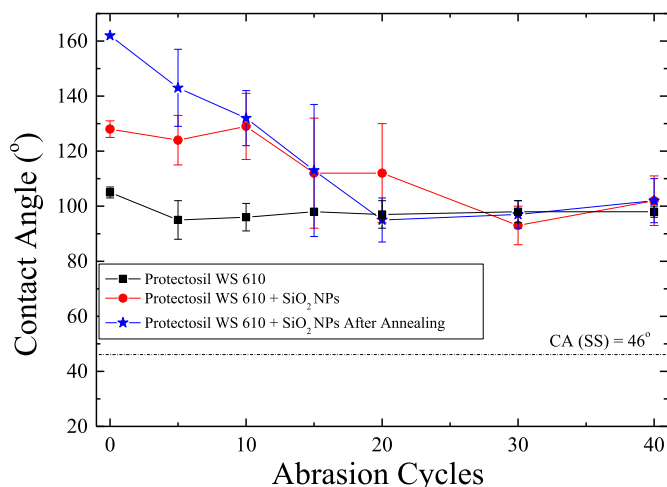


Fig. 10. Water contact angle values as a function of abrasion cycles (sandpaper test) for Protectosil® WS 610 (black squares) and for a nanocomposite coating with 70 wt% Protectosil® WS 610 and 30 wt% SiO₂ before (red circles) and after (blue stars) thermal annealing. The dotted line indicates the water contact angle for the neat stainless steel substrate. (For interpretation of the references to colour in this figure legend, the reader is referred to the Web version of this article.)

after more abrasion cycles, a gradual yet significant decrease is observed and beyond ~20 cycles the contact angle values become similar to those of the pure Protectosil® coatings, reaching approximately 100° (red circles and blue stars). These results suggest that abrasion can affect the polymeric Protectosil® coatings to a very limited extent, while considerably degrades the nanocomposite ones. Under mechanical stress, the SiO₂ based hybrid coating steadily loses both its superhydrophobicity and its water-repellence, showing a rather poor mechanical durability compared to that of the pure polymer. Similar experiments were conducted using an abrasion tester with a microfiber coated tool and a load of 420 g for a total of up to 2500 abrasion cycles. The results were consistent with those described above, confirming that the degradation of the surface properties of the coatings occurs within the initial abrasion cycles, after which the coatings remain stable (Fig. S7).

To investigate the impact of abrasion on a surface that was originally

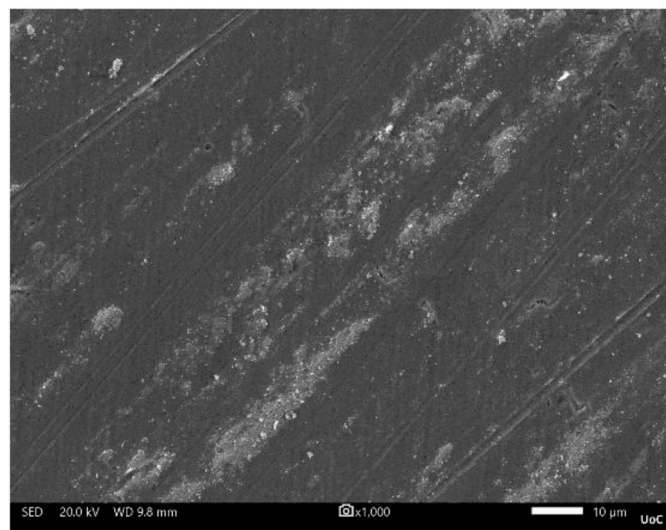


Fig. 11. SEM image of a 70 wt% Protectosil® WS 610 + 30 wt% SiO₂ coating on a stainless steel substrate, after thermal annealing and subsequent abrasion testing with sandpaper (40 cycles). This image was taken with a magnification of $\times 100$, whereas the scale bar corresponds to 10 μ m.

displaying water-repellent properties, SEM imaging was performed. Fig. 11 clearly shows the removal of surface particles by the abrasion test, while it also reveals noticeable damage of the surface and linear scratches induced by the rubbing action. This is further reflected by EDS analysis (Table S5), which confirms a loss in the Si signal with a corresponding increase in Fe and Cr, coming from the stainless steel substrate.

The average EDS results are consistent with the respective elemental mapping, which also reveals a significant loss of coating material, as smaller quantities of C, O and Si are still detectable on the surface in comparison with the coated surface before abrasion (Fig. S8). In conclusion, the SiO₂ particles are gradually removed from the surface during the abrasion because of their poor adhesion to the polymer matrix and the substrate. The mechanical durability of superhydrophobic coatings is still an open problem even for the coatings containing fluorinated compounds.

Contrary to the results obtained from the mechanical durability tests, chemical durability tests showed a completely stable behavior. In this regard, neat Protectosil® WS 610 coatings as well as Protectosil® nanocomposite coatings with SiO₂ nanoparticles, both thermally annealed, were exposed to aqueous solutions at extreme pH values, such as pH 2 and pH 13, as well as at neutral conditions (pH 7), to investigate their stability against chemically harsh environments. Fig. 12 shows water contact angles for coatings that remained at these conditions for different time intervals; for the first 5 h, measurements were performed every hour while for longer tests every 5 h until a total duration of 15 h was reached. Evidently, no change in the contact angles could be detected even after 15 h-long immersion in the case of polymeric coatings. More importantly, the nanocomposite coatings remained superhydrophobic and water-repellent even after long exposure under such harsh conditions. This should be attributed to the notable chemical stability of the strong Si–O bonds of the silicon-based network that is formed, whereas the hydrophobic organic side groups remain exposed but are inert to H⁺ and OH[−] ions, providing exceptional resilience under both acidic and alkaline conditions. This combination allows the surface to remain superhydrophobic and water-repellent behavior over exposure time [74].

In the present work, superhydrophobic, water-repellent, chemically stable and cytocompatible coatings that do not contain any fluoropolymers were developed. The proposed strategy includes a single-step method for the preparation of the coating formulation, followed by a simple spray deposition process. The approach is low-cost, very simple,

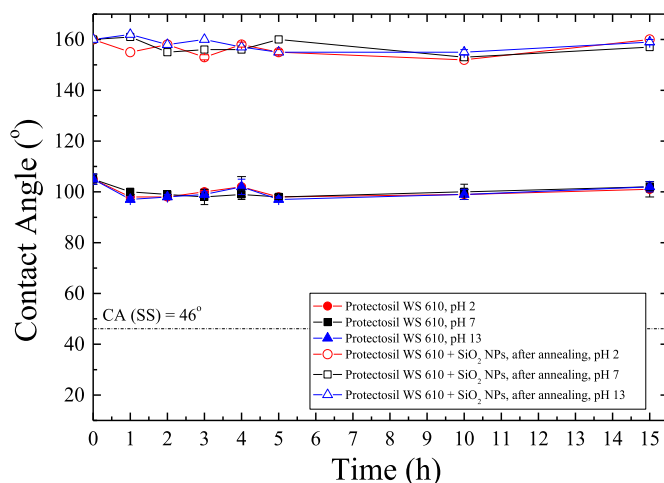


Fig. 12. Water contact angle values as a function of exposure time in acidic (pH 2, red circles), neutral (pH 7, black squares) and basic (pH 13, blue triangles) aqueous solutions for the Protectosil® coating (filled symbols) and the thermally annealed nanocomposite Protectosil®-based coatings with 30 wt% SiO₂ nanoparticles (open symbols). (For interpretation of the references to colour in this figure legend, the reader is referred to the Web version of this article.)

scalable and easy to be applied by non-experienced personnel even over large surfaces. However, achieving mechanical durability of the coatings is still a complex materials engineering challenge that requires further research.

4. Conclusions

Environmentally friendly superhydrophobic and water-repellent as well as cytocompatible nanocomposite coatings were successfully developed based on Protectosil® WS 610, a new non-fluorinated silicone-based polymer, and SiO₂ nanoparticles. The neat polymer coatings exhibited water contact angles of approximately 100° with very low hysteresis (~10°), indicating low water adhesion and stable surface behavior. To further enhance the apparent hydrophobicity of the surface, SiO₂ nanoparticles were incorporated into the polymer matrix to develop nanocomposite coatings with the appropriate roughness. For nanoparticle concentrations in the range 30 – 50 wt%, the coatings exhibited contact angles above 120°, demonstrating improved hydrophobic performance, however, with high water adhesion. Nevertheless, when these nanohybrid coatings were annealed at 65 °C for 24 h, a significant improvement in the wetting properties was observed with the coatings exhibiting superhydrophobic and water-repellent behavior highlighting the role of mild thermal treatment in optimizing the homogeneity of the surface roughness. Cytocompatibility assessment confirmed that all coatings were safe and suitable for applications with human involvement. Moreover, chemical durability tests showed that both the polymeric and annealed nanocomposite coatings remain stable even under extreme acidic or basic pH conditions. On the other hand, mechanical tests revealed that the pure Protectosil® coatings can withstand several abrasion cycles, whereas the nanocomposite coatings lose their superhydrophobic and water-repellent properties under mechanical stress.

Mechanical durability is a key issue for the development of sustainable superhydrophobic and water-repellent coatings with long lifetime. The loss of the superhydrophobicity that we also observed in the current work is mostly related to the SiO₂ particles gradually being removed from the surface during the abrasion cycles probably because of their poor adhesion to the polymer matrix and the substrate. A key challenge is, therefore, the improvement of the interaction and the bonding between the silanol groups of the matrix, on one hand, and the hydroxyl groups of the silica nanoparticles and of the various substrates on the other, which will, thus, form a stronger siloxane network providing enhanced adhesion. In principle, this may be enhanced by using an extra “binder” in the formulation, which, however, may influence the water-repellent properties of the coating or its cytocompatibility. Note that the mechanical durability of superhydrophobic coatings is still an open problem even for coatings containing fluorinated compounds. In certain cases, an extra processing step has been proposed that introduces an “adhesion layer” that may improve adhesion of the coating to the substrate. This, however, not only introduces an extra processing step but, also, it cannot ensure the good adhesion of the matrix to the nanoparticles, which provide the appropriate roughness to the coating. Therefore, the question of mechanical durability of the coatings requires further investigation.

Overall, this work presents a simple, non-toxic, and effective strategy to replace fluorinated materials with safer alternatives, using nanohybrid coatings that consist of silicone polymers and nanoparticles to achieve high-performance superhydrophobic and water-repellent surfaces.

CRediT authorship contribution statement

Erta Petsi: Writing – original draft, Validation, Methodology, Investigation, Data curation. **Franceska Gojda:** Methodology, Investigation, Data curation. **Fanourios Krasanakis:** Writing – review & editing, Validation, Supervision. **Abeer Shaalan:** Validation,

Methodology, Investigation, Data curation. **Minas M. Stylianakis:** Writing – review & editing, Validation, Supervision. **Lucy Di Silvio:** Validation, Supervision. **Kiriaki Chrissopoulou:** Writing – review & editing, Validation, Supervision, Project administration. **Spiros H. Anastasiadis:** Writing – review & editing, Validation, Supervision, Resources, Conceptualization.

Declaration of competing interest

The authors declare the following financial interests/personal relationships which may be considered as potential competing interests: Spiros H. Anastasiadis reports financial support was provided by EU Horizon Europe. He and the other authors declare that they have no known competing financial interests or personal relationships that could have appeared to influence the work reported in this paper.

Acknowledgements

This research has been financed by EU Horizon Europe Programme (project STOP, Grant Agreement 101057961). The authors acknowledge the help of Dr. Athanasios Kostopoulos with the profilometry measurements, of Mrs. Katerina Tsagaraki with the AFM measurements, of Mr. Stefanos Papadakis and Mrs. Aleka Manousaki with the SEM/EDS measurements, and of Katerina Stamataki for the IR measurement. We also acknowledge Dr. Vasileios Tzatzadakis for the creation of the Graphical Abstract using BioRender.

Appendix. ASupplementary data

Supplementary data to this article can be found online at <https://doi.org/10.1016/j.polymer.2026.129851>.

Data availability

Data will be made available on request.

References

- [1] S.G. Moghadam, H. Parsimehr, A. Ehsani, Multifunctional superhydrophobic surfaces, *Adv. Colloid Interface Sci.* 290 (2021) 102397, <https://doi.org/10.1016/j.cis.2021.102397>.
- [2] J.T. Simpson, S.R. Hunter, T. Aytug, Superhydrophobic materials and coatings: a review, *Rep. Prog. Phys.* 78 (2015) 086501, <https://doi.org/10.1088/0034-4885/78/8/086501>.
- [3] N.J. Shirtcliffe, G. McHale, S. Atherton, M.I. Newton, An introduction to superhydrophobicity, *Adv. Colloid Interface Sci.* 161 (2010) 124–138, <https://doi.org/10.1016/j.cis.2009.11.001>.
- [4] M. Barberoglou, V. Zorba, E. Stratakis, E. Spanakis, P. Tzanetakis, S. H. Anastasiadis, C. Fotakis, Bio-inspired water repellent surfaces produced by ultrafast laser structuring of silicon, *Appl. Surf. Sci.* 225 (2009) 5425–5429, <https://doi.org/10.1016/j.apsusc.2008.07.130>.
- [5] I.P. Parkin, R.G. Palgrave, Self-cleaning coatings, *J. Mater. Chem.* 15 (2005) 1689–1695, <https://doi.org/10.1039/B412803F>.
- [6] B. Bhushan, Y.C. Jung, K. Kerstin, Self-cleaning efficiency of artificial superhydrophobic surfaces, *Langmuir* 25 (2009) 3240–3248, <https://doi.org/10.1021/la803860d>.
- [7] K. Liu, J. Lei, Bio-inspired self-cleaning surfaces, *Annu. Rev. Mater. Res.* 42 (2012) 231–263, <https://doi.org/10.1146/annurev-matsci-070511-155046>.
- [8] A. Nurioglu, C. Esteves, Gijbertus de With, Non-toxic, non-biocide-release antifouling coatings based on molecular structure design for marine applications, *J. Mater. Chem. B* 3 (2015) 6547–6570, <https://doi.org/10.1039/C5TB00232J>.
- [9] Z. He, X. Lan, Q. Hu, H. Li, L. Li, J. Mao, Antifouling strategies based on superphobic polymer materials, *Prog. Org. Coating* 157 (2021) 106285, <https://doi.org/10.1016/j.porgcoat.2021.106285>.
- [10] L. Gao, C. Andrew, K. Wu Di, J. Vinod, K.S. Jianzhong, Anti-icing superhydrophobic coatings, *Langmuir* 25 (2009) 12444–12448, <https://doi.org/10.1021/la902882b>.
- [11] M.J. Kreder, J. Alvarenga, P. Kim, J. Aizenberg, Design of anti-icing surfaces: smooth, textured or slippery? *Nat. Rev. Mater.* 1 (2016) 15003 <https://doi.org/10.1038/natrevmats.2015.3>.
- [12] B.L. Boinovich, A.G. Domantovskii, A.M. Emelyanenko, A.B. Miller, Y.F. Potapov, A.N. Khodan, Anticing performance of superhydrophobic coatings on aluminum and stainless steel, *Russ. Chem. Bull.* 62 (2013) 380–387, <https://doi.org/10.1007/s11172-013-0049-6>.

- [13] D.W. Wei, H. Wei, A.C. Gauthier, J. Song, Y. Jin, H. Xiao, Superhydrophobic modification of cellulose and cotton textiles: methodologies and applications, *J. Bioresour. Bioprod.* 5 (2020) 1–15, <https://doi.org/10.1016/j.jobab.2020.03.001>.
- [14] H. Xinting, X. Gong, In situ, one-pot method to prepare robust superamphiphobic cotton fabrics for high buoyancy and good antifouling, *ACS Appl. Mater. Interfaces* 13 (2021) 31298–31309, <https://doi.org/10.1021/acsami.1c08844>.
- [15] P. Chauhan, A. Kumar, B. Bhushan, Self-cleaning, stain-resistant and anti-bacterial superhydrophobic cotton fabric prepared by simple immersion technique, *J. Colloid Interface Sci.* 535 (2019) 66–74, <https://doi.org/10.1016/j.jcis.2018.09.087>.
- [16] J. Lomga, P. Varshney, D. Nanda, M. Satapathy, S.S. Mohapatra, A. Kumar, Fabrication of durable and regenerable superhydrophobic coatings with excellent self-cleaning and anti-fogging properties for aluminium surfaces, *J. Alloys Compd.* 702 (2017) 161–170, <https://doi.org/10.1016/j.jallcom.2017.01.243>.
- [17] I. Fatimah, A.R. Bushroa, S. Wee, Fundamentals of antifogging strategies, coating techniques and properties of inorganic materials; a comprehensive review, *J. Mater. Res. Technol.* 23 (2023) 687–714, <https://doi.org/10.1016/j.jmrt.2023.01.015>.
- [18] J. Yoon, M. Ryu, H. Kim, G.N. Ahn, S.J. Yim, D.P. Kim, H. Lee, Wet-style superhydrophobic antifogging coatings for optical sensors, *Adv. Mater.* 32 (2020) 2002710, <https://doi.org/10.1002/adma.202002710>.
- [19] N.M. Oliveira, A.I. Neto, W. Song, J.F. Mano, Two-dimensional open microfluidic devices by tuning the wettability on patterned superhydrophobic polymeric surface, *Appl. Phys. Express* 3 (2010) 085205, <https://doi.org/10.1143/APEX.3.085205>.
- [20] M.C. Draper, C.R. Crick, V. Orlickaite, V.A. Turek, I.P. Parkin, J.B. Edel, Superhydrophobic surfaces as an on-chip microfluidic toolkit for total droplet control, *Anal. Chem.* 85 (2013) 5405–5410, <https://doi.org/10.1021/ac303786s>.
- [21] Y. Wanchen, Y. Yan, J. Sun, Z. Zhang, W. Sun, W. Huang, J. Cheng, H. Zhao, M. Xie, Q. Sun, G. Huang, X. Lin, Mechanically durable superhydrophobic strain sensors with high biocompatibility and sensing performance for underwater motion monitoring, *ACS Appl. Mater. Interfaces* 16 (2024) 6548–6561, <https://doi.org/10.1021/acsami.3c14327>.
- [22] W. Yenyu, C.-N. Lai, C.-C. Yen, X. Jiang, D. Peroulis, Lia A. Stanciu, Surface functionalization of Ti3C2Tx MXene with highly reliable superhydrophobic protection for volatile organic compounds sensing, *ACS Nano* 14 (2020) 11490–11501, <https://doi.org/10.1021/acsnano.0c03896>.
- [23] S.T. Yohe, Y.L. Colson, M.W. Grinstaff, Superhydrophobic materials for tunable drug release: using displacement of air to control delivery rates, *J. Am. Chem. Soc.* 134 (2012) 2016–2019, <https://doi.org/10.1021/ja211148a>.
- [24] S.H. Anastasiadis, Development of functional polymer surfaces with controlled wettability, *Langmuir* 29 (2013) 9277–9290, <https://doi.org/10.1021/la400533u>.
- [25] S.W. Jiang, K.L. Yao, X. Lei, Bioinspired surfaces with superwettability: new insight on theory, design, and applications, *Chem. Rev.* 115 (2015) 8230–8293, <https://doi.org/10.1021/cr400083v>.
- [26] B. Bhushan, Y.C. Jung, K. Koch, Micro-, nano- and hierarchical structures for superhydrophobicity, self-cleaning and low adhesion, *Philos. Trans. R. Soc. A Math. Phys. Eng. Sci.* 367 (2009) 1631–1672, <https://doi.org/10.1098/rsta.2009.0014>.
- [27] V. Zorba, E. Stratakis, M. Barberoglou, E. Spanakis, P. Tzanetakis, S. H. Anastasiadis, C. Fotakis, Biomimetic artificial surfaces quantitatively reproduce the water repellency of a lotus leaf, *Adv. Mater.* 20 (2008) 4049–4054, <https://doi.org/10.1002/adma.200800651>.
- [28] A. Marmur, The lotus effect: superhydrophobicity and metastability, *Langmuir* 20 (2004) 3517–3519, <https://doi.org/10.1021/la036369u>.
- [29] W. Barthlott, C. Neinhuis, Purity of the sacred lotus, or escape from contamination in biological surfaces, *Planta* 202 (1997) 1–8, <https://doi.org/10.1007/s004250050096>.
- [30] R.D. Mukhopadhyay, B. Vedhanarayanan, A. Ajayaghosh, Creation of “rose petal” and “lotus leaf” effects on alumina by surface functionalization and metal-ion coordination, *Angew. Chem. Int. Ed.* 56 (2017) 16018–16022, <https://doi.org/10.1002/anie.201709463>.
- [31] H.M.K. Dawood, T.H. Zheng, K.C. Liew, Y.L. Leong, R. Foo, S.A. Rajagopalan, W. K. Khan Choi, Mimicking both petal and lotus effects on a single silicon substrate by tuning the wettability of nanostructured surfaces, *Langmuir* 27 (2011) 4126–4133, <https://doi.org/10.1021/la1050783>.
- [32] M.J. Nine, T.T. Tung, F. Alotaibi, D.N.H. Tran, D. Losic, Facile adhesion-tuning of superhydrophobic surfaces between “lotus” and “petal” effect and their influence on icing and deicing properties, *ACS Appl. Mater. Interfaces* 9 (2017) 8393–8402, <https://doi.org/10.1021/acsami.6b16444>.
- [33] R. Sun, J. Zhao, Z. Li, N. Qin, J. Mo, Y.J. Pan, D. Luo, Robust superhydrophobic aluminum alloy surfaces with anti-icing ability, thermostability, and mechanical durability, *Prog. Org. Coating* 147 (2020) 105745, <https://doi.org/10.1016/j.porgcoat.2020.105745>.
- [34] J. Feng, M.T. Tuominen, J.P. Rothstein, Hierarchical superhydrophobic surfaces fabricated by dual-scale electron-beam-lithography with well-ordered secondary nanostructures, *Adv. Funct. Mater.* 21 (2011) 3715–3722, <https://doi.org/10.1002/adfm.201100665>.
- [35] Q. Pan, Y. Cao, W. Xue, D. Zhu, W. Liu, Picosecond laser-textured stainless steel superhydrophobic surface with an antibacterial adhesion property, *Langmuir* 35 (2019) 11414–11421, <https://doi.org/10.1021/acs.langmuir.9b01333>.
- [36] F. Gojda, M. Loulakis, L. Papoutsakis, S. Tzortzakakis, K. Chrissopoulou, S. H. Anastasiadis, Altering the surface properties of metal alloys utilizing facile and ecological methods, *Langmuir* 38 (2022) 4826–4838, <https://doi.org/10.1021/acs.langmuir.1c03431>.
- [37] F. Krasanakis, T.M. Chatzaki, K. Chrissopoulou, S.H. Anastasiadis, Modifying flexible polymer films towards superhydrophobicity and superoleophobicity by utilizing water-based nanohybrid coatings, *Nanoscale* 15 (2023) 6984–6998, <https://doi.org/10.1039/d2nr06780c>.
- [38] Y. Wu, S. Jia, Y. Qing, S. Luo, M. Liu, A versatile and efficient method to fabricate durable superhydrophobic surfaces on wood, lignocellulosic fiber, glass, and metal substrates, *J. Mater. Chem. A* 4 (2016) 14111–14121, <https://doi.org/10.1039/c6ta05259b>.
- [39] P.N. Manoudis, A. Tsakalof, I. Karapanagiotis, I. Zuburtikudis, C. Panayiotou, Fabrication of super-hydrophobic surfaces for enhanced stone protection, *Surf. Coat. Technol.* 203 (2009) 1322–1328, <https://doi.org/10.1016/j.surfcoat.2008.10.041>.
- [40] F. Gojda, A. Thomos, F. Krasanakis, M.M. Stylianakis, K. Chrissopoulou, S.H. Anastasiadis, Superhydrophobic and water-repellent coatings with dual-scale roughness based on MXene/polymer nanocomposites, *ACS Appl. Mater. Interfaces*, submitted for publication.
- [41] I. Boticas, D. Dias, D. Ferreira, P. Magalhães, R. Silva, R. Figueiro, Superhydrophobic cotton fabrics based on ZnO nanoparticles functionalization, *SN Appl. Sci.* 1 (2019) 1–9, <https://doi.org/10.1007/s42452-019-1423-2>.
- [42] M. Shaban, F. Mohamed, S. Abdallah, Production and characterization of superhydrophobic and antibacterial coated fabrics utilizing ZnO nanocatalyst, *Sci. Rep.* 8 (2018) 1–15, <https://doi.org/10.1038/s41598-018-22324-7>.
- [43] M.M. Rashid, B. Simončić, B. Tomšič, Recent advances in TiO₂-functionalized textile surfaces, *Surf. Interfaces* 22 (2021) 1–33, <https://doi.org/10.1016/j.surfint.2020.100890>.
- [44] C.H. Han, B.G. Min, Superhydrophobic and antibacterial properties of cotton fabrics coated with copper nanoparticles through sonochemical process, *Fibers Polym.* 21 (2020) 785–791, <https://doi.org/10.1007/s12221-020-9925-5>.
- [45] L. Gao, Y. Lu, J. Li, Q. Sun, Superhydrophobic conductive wood with oil repellency obtained by coating with silver nanoparticles modified by fluoroalkyl silane, *Holzschung* 70 (2016) 63–68, <https://doi.org/10.1515/hf-2014-0226>.
- [46] B. Zhang, W. Xu, Q. Zhu, B. Hou, Scalable, fluorine free and hot water repelling superhydrophobic and superoleophobic coating based on functionalized Al₂O₃ nanoparticles, *J. Mater. Sci. Technol.* 66 (2021) 74–81, <https://doi.org/10.1016/j.jmst.2020.06.035>.
- [47] A. Bake, M. Merah, A. Matin, M. Gondal, T. Qahtan, N. Abu-Dheir, Preparation of transparent and robust superhydrophobic surfaces for self-cleaning applications, *Prog. Org. Coating* 122 (2018) 170–179, <https://doi.org/10.1016/j.porgcoat.2018.05.018>.
- [48] Y.S. Cho, S. Nam, S. Jeong, Y.S. Kim, Low-cost fabrication of flexible water-repellent film by spray coating of a hydrophobic nanoparticle dispersion, *J. Dispersion Sci. Technol.* 41 (2020) 1526–1539, <https://doi.org/10.1080/01932691.2019.1627883>.
- [49] J. Zhang, B. Li, L. Wu, A. Wang, Facile preparation of durable and robust superhydrophobic textiles by dip coating in nanocomposite solution of organosilanes, *Chem. Commun.* 49 (2013) 11509–11511, <https://doi.org/10.1039/c3cc43238f>.
- [50] B.K. Nandi, R. Uppaluri, M.K. Purkait, Effects of dip coating parameters on the morphology and transport properties of cellulose acetate-ceramic composite membranes, *J. Membr. Sci.* 330 (2009) 246–258, <https://doi.org/10.1016/j.memsci.2008.12.071>.
- [51] M.S. Han, Y. Park, C.H. Park, Development of superhydrophobic polyester fabrics using alkaline hydrolysis and coating with fluorinated polymers, *Fibers Polym.* 17 (2016) 241–247, <https://doi.org/10.1007/s12221-016-5693-7>.
- [52] M. Yang, W. Liu, C. Jiang, S. He, Y. Xie, Z. Wang, Fabrication of superhydrophobic cotton fabric with fluorinated TiO₂ sol by a green and one-step sol-gel process, *Carbohydr. Polym.* 197 (2018) 75–82, <https://doi.org/10.1016/j.carbpol.2018.05.075>.
- [53] T.M. Schutzius, I.S. Bayer, M.K. Tiwari, C.M. Megaridis, Novel fluoropolymer blends for the fabrication of sprayable multifunctional superhydrophobic nanostructured composites, *Ind. Eng. Chem. Res.* 50 (2011) 11117–11123, <https://doi.org/10.1021/ie200814r>.
- [54] P. Khanjani, A.W.T. King, G.J. Partl, L.-S. Johansson, M.A. Kostianen, R.H.A. Ras, Superhydrophobic paper from nanostructured fluorinated cellulose esters, *ACS Appl. Mater. Interfaces* 10 (2018) 11280–11288, <https://doi.org/10.1021/acsami.7b19310>.
- [55] S. Desbief, B. Grignard, C. Detrembleur, R. Rioboo, A. Vaillant, D. Severno, M. Voué, J. De Coninck, A.M. Jonas, C. Jérôme, P. Damman, R. Lazzaroni, Superhydrophobic aluminum surfaces by deposition of micelles of fluorinated block copolymers, *Langmuir* 26 (2010) 2057–2067, <https://doi.org/10.1021/la902565y>.
- [56] H. Li, Y. Zhao, X. Yuan, Facile preparation of superhydrophobic coating by spraying a fluorinated acrylic random copolymer micelle solution, *Soft Matter* 9 (2013) 1005–1009, <https://doi.org/10.1039/c2sm26689j>.
- [57] Q. Li, Y. Yan, M. Yu, B. Song, S. Shi, Y. Gong, Synthesis of polymeric fluorinated sol-gel precursor for fabrication of superhydrophobic coating, *Appl. Surf. Sci.* 367 (2016) 101–108, <https://doi.org/10.1016/j.apsusc.2016.01.155>.
- [58] M.A. Miller, E.M. Sletten, Perfluorocarbons in chemical biology, *Chembiochem* 21 (2020) 3451–3462, <https://doi.org/10.1002/cbic.202000297>.
- [59] S.E. Fenton, A. Ducatman, A. Boobis, J.C. DeWitt, C. Lau, C. Ng, J.S. Smith, S. M. Roberts, Per- and polyfluoroalkyl substance toxicity and human health review: current state of knowledge and strategies for informing future research, *Environ. Toxicol. Chem.* 40 (2021) 606–630, <https://doi.org/10.1002/etc.4890>.
- [60] L.J.L. Espartero, M. Yamada, J. Ford, G. Owens, T. Prow, A. Juhasz, Health-related toxicity of emerging per- and polyfluoroalkyl substances: Comparison to legacy

- PFOS and PFOA, *Environ. Res.* 212 (2022) 113431, <https://doi.org/10.1016/j.envres.2022.113431>.
- [61] S. Ullah, S. Ahmad, X. Guo, S. Ullah, S. Ullah, G. Nabi, K. Wanghe, A review of the endocrine disrupting effects of micro and nano plastic and their associated chemicals in mammals, *Front. Endocrinol. (Lausanne)*. 13 (2023), <https://doi.org/10.3389/fendo.2022.1084236>.
- [62] N.R. Binczewski, L.M. Morimoto, J.L. Wiemels, X. Ma, C. Metayer, V.M. Vieira, Prenatal exposure to per- and polyfluoroalkyl substances (PFAS) from contaminated water and risk of childhood cancer in California, 2000–2015, *Environ. Epidemiol.* 9 (2025) e365, <https://doi.org/10.1097/EE9.0000000000000365>.
- [63] A. Biggeri, G. Stoppa, L. Facciolo, G. Fin, S. Mancini, V. Manno, G. Minelli, F. Zamagni, M. Zamboni, D. Catelan, L. Bucchi, All-cause, cardiovascular disease and cancer mortality in the population of a large Italian area contaminated by perfluoroalkyl and polyfluoroalkyl substances (1980–2018), *Environ. Health* 23 (2024) 42, <https://doi.org/10.1186/s12940-024-01074-2>.
- [64] A. Perez, M. Lumpkin, T. Kornberg, A. Schmidt, Critical endpoints of PFOA and PFOS exposure for regulatory risk assessment in drinking water: parameter choices impacting estimates of safe exposure levels, *Regul. Toxicol. Pharmacol.* 138 (2023) 105323, <https://doi.org/10.1016/j.yrtph.2022.105323>.
- [65] S. Kurwadkar, J. Dane, S.R. Kanel, M.N. Nadagouda, R.W. Cawdrey, B. Ambade, G. C. Struckhoff, R. Wilkin, Per- and polyfluoroalkyl substances in water and wastewater: a critical review of their global occurrence and distribution, *Sci. Total Environ.* 809 (2022) 151003, <https://doi.org/10.1016/j.scitotenv.2021.151003>.
- [66] J.L. Domingo, M. Nadal, Human exposure to per- and polyfluoroalkyl substances (PFAS) through drinking water: a review of the recent scientific literature, *Environ. Res.* 177 (2019) 108648, <https://doi.org/10.1016/j.envres.2019.108648>.
- [67] D. Savoca, A. Pace, Bioaccumulation, biodistribution, toxicology and biomonitoring of organofluorine compounds in aquatic organisms, *Int. J. Mol. Sci.* 22 (2021) 6276, <https://doi.org/10.3390/ijms22126276>.
- [68] G. Ding, W. Peijnenburg, Physicochemical properties and aquatic toxicity of poly- and perfluorinated compounds, *Crit. Rev. Environ. Sci. Technol.* 43 (2013) 598–678, <https://doi.org/10.1080/10643389.2011.627016>.
- [69] J. Han, L. Kiss, H. Mei, A.M. Remete, M. Ponikvar-Svet, D.M. Sedgwick, R. Roman, S. Fustero, H. Moriwaki, V.A. Soloshonok, Chemical aspects of human and environmental overload with fluorine, *Chem. Rev.* 121 (2021) 4678–4742, <https://doi.org/10.1021/acs.chemrev.0c01263>.
- [70] Q. Wang, G. Sun, Q. Tong, W. Yang, W. Hao, Fluorine-free superhydrophobic coatings from polydimethylsiloxane for sustainable chemical engineering : preparation methods and applications, *Chem. Eng. J.* 426 (2021) 130829, <https://doi.org/10.1016/j.cej.2021.130829>.
- [71] S. Gao, X. Dong, J. Huang, S. Li, Y. Li, Z. Chen, Y. Lai, Rational construction of highly transparent superhydrophobic coatings based on a non-particle, fluorine-free and water-rich system for versatile oil-water separation, *Chem. Eng. J.* 333 (2018) 621–629, <https://doi.org/10.1016/j.cej.2017.10.006>.
- [72] H. He, W. Huang, Z. Guo, Superhydrophobic and photothermal SiC/TiN durable composite coatings for passive anti-icing/active de-icing and de-frosting, *Mater. Today Phys.* 30 (2023) 100927, <https://doi.org/10.1016/j.mtphys.2022.100927>.
- [73] W. Song, H. Song, Z. Fan, S. Cheng, Z. Feng, Preparation of robust fluorine-free superhydrophobic coating using fly ash and its self-cleaning, anti-icing and anti-corrosion properties, *Surf. Coat. Technol.* 513 (2025) 132480, <https://doi.org/10.1016/j.surfcoat.2025.132480>.
- [74] H. Li, X. Wu, Z. Tang, M. Zhang, Z. Zheng, Y. Liu, One-step biomimetic construction of bio-based, robust and superhydrophobic coatings for simultaneously enhancing the surface functionality and passive fire-proof of steel structures, *Constr. Build. Mater.* 496 (2025) 143815, <https://doi.org/10.1016/j.conbuildmat.2025.143815>.
- [75] Z. Tang, M. Gao, H. Li, Z. Zhang, X. Su, Y. Li, Z. Han, X. Lv, J. He, Z. Zheng, Y. Liu, Facile and effective construction of superhydrophobic, multi-functional and durable coatings on steel structure, *Compos. Part B Eng.* 287 (2024) 111850, <https://doi.org/10.1016/j.compositesb.2024.111850>.
- [76] R.A. Sathya, C. Ponraj, Non-fluorinated, anti-reflective, self-cleaning and durable silane based superhydrophobic coating for floating solar cells, *Mater. Chem. Phys.* 341 (2025) 130880, <https://doi.org/10.1016/j.matchemphys.2025.130880>.
- [77] C. Cao, M. Ge, J. Huang, S. Li, S. Deng, S. Zhang, Z. Chen, K. Zhang, S.S. Al-Deyab, Y. Lai, Robust fluorine-free superhydrophobic PDMS-ormosil@fabrics for highly effective self-cleaning and efficient oil-water separation, *J. Mater. Chem. A* 4 (2016) 12179–12187, <https://doi.org/10.1039/c6ta04420d>.
- [78] Y. Luo, S. Wang, X. Fu, X. Du, H. Wang, X. Cheng, Z. Du, Preparation of fluorine-free superhydrophobic and wear-resistant cotton fabric with a UV curing reaction for self-cleaning and oil/water separation, *RSC Adv.* 11 (2021) 4660–4671, <https://doi.org/10.1039/d0ra10060a>.
- [79] Z. Zhang, X. Fang, Y. Meng, Y. Xu, X. Wang, H. Niu, H. Zhou, A cavitated-ridged reentrant coating system for fabrication of robust, fluorine-free superomniphobic surfaces, *Small* 21 (2025), <https://doi.org/10.1002/smll.202507869>.
- [80] N. Agrawal, P.S. Low, J.S.J. Tan, E.W.M. Fong, Y. Lai, Z. Chen, Durable easy-cleaning and antibacterial cotton fabrics using fluorine-free silane coupling agents and CuO nanoparticles, *Nano Mater. Sci.* 2 (2020) 281–291, <https://doi.org/10.1016/j.nanoms.2019.09.004>.
- [81] J.J. Kalmoni, C.S. Blackman, C.J. Carmalt, Tuneable wetting of fluorine-free superhydrophobic films via titania modification to enhance durability and photocatalytic activity, *Adv. Mater. Interfac.* 11 (2024) 2400519, <https://doi.org/10.1002/admi.202400519>.
- [82] V. Diniz, N.M. Pugno, S. Rath, C.R. Crick, The fabrication of fluorine-free stretchable superhydrophobic films using inverse vulcanization sulfur polymer, *Adv. Mater. Interfac.* 12 (2025) 2400896, <https://doi.org/10.1002/admi.202400896>.
- [83] B. John, S.K. Sahoo, Development of nanofree, silane-free, and fluorine-free cardanol-based multifunctional, superhydrophobic wood coating, *ACS Appl. Polym. Mater.* 6 (2024) 9226–9237, <https://doi.org/10.1021/acsapm.4c01640>.
- [84] J. Coates, Interpretation of infrared spectra, A practical approach, in: R.A. Meyers, M.L. McKelvy (Eds.), *Encyclopedia of Analytical Chemistry*, 2000, <https://doi.org/10.1002/9780470027318.a5606>.
- [85] P.J. Launer, Infrared analysis of organosilicon compounds: spectra-structure correlations, in: B. Arkles, G. Larson (Eds.), *Silicon Compounds: Silanes & Silicenes*, Gelest, Inc., Morrisville, PA, 2013, pp. 175–178.
- [86] A.G. Milekhin, C. Himcinschi, M. Friedrich, K. Hiller, M. Wiemer, T. Gessner, S. Schulze, D.R.T. Zahn, Infrared spectroscopy of bonded silicon wafers, *Semiconductors* 40 (2006) 1304–1313, <https://doi.org/10.1134/S1063782606110108>.
- [87] B.C. Smith, Inorganics III, Even more spectra, and the grand finale, *Spectrosc. (St. Monica)* 39 (2024) 11–15, <https://doi.org/10.56530/spectroscopy.hp2485x8>.